Preface to the Book Series

To train young people to grind lenses… . I cannot see there would be much use…because most students go there to make money out of science or to get a reputation in the learned world. But in lens-grinding and discovering things hidden from our sight, these count for nought.

—Antonie van Leeuwenhoek

Letter to Gottfried Leibniz on 28 September 1715 in response to Leibniz' request that he should open a school to train young people in microscopy

You can observe a lot just by watching.

—Yogi Berra

ONE OF THE CENTRAL THEMES OF BIOLOGY IS the constant change and transformation of most biological systems. In fact, this dynamic aspect of biology is one of its most fascinating characteristics, and it draws generation after generation of students absorbed in understanding how an organism develops, how a cell functions, or how the brain works. This series of manuals covers imaging techniques in the life sciences—techniques that try to capture these dynamics. The application of optical and other visualization techniques to study living organisms constitutes a direct methodology to follow the form and the function of cells and tissues by generating two- or three-dimensional images of them and to document their dynamic nature over time. Although it seems natural to use light to study cells or tissues, and microscopists have been doing this with fixed preparations since van Leeuwenhoek's time, the imaging of living preparations has only recently become standard practice. It is not an overstatement to say that imaging technologies have revolutionized research in many areas of biology and medicine. In addition to advances in microscopy, such as differential interference contrast or the early introduction of video technology and digital cameras, the development of methods to culture cells, to keep tissue slices alive, and to maintain living preparations, even awake and behaving, on microscopes has opened new territories to biologists. The synthesis of novel fluorescent tracers, indicator dyes, and nanocrystals and the explosive development of fluorescent protein engineering, optogenetical constructs, and other optical actuators like caged compounds have made possible studies characterizing and manipulating the form and function of cells, tissues, and circuits with unprecedented detail, from the single-molecule level to that of an entire organism. A similar revolution has occurred on the optical design of microscopes. Originally, confocal microscopy became the state-of-the-art imaging approach because of its superb spatial resolution and three-dimensional sectioning capabilities; later, the development of two-photon excitation enabled fluorescence imaging of small structures in the midst of highly scattered living media, such as whole-animal preparations, with increased optical penetration and reduced photodamage. Other

nonlinear optical techniques, such as second-harmonic generation and coherent anti-Stokes Raman scattering (CARS), now follow and appear well suited for measurements of voltage and biochemical events at interfaces such as plasma membranes. Finally, an entire generation of novel "superresolution" techniques, such as stimulated emission depletion (STED), photoactivated localization microscopy (PALM), and stochastic optical reconstruction microscopy (STORM), has arisen. These techniques have broken the diffraction limit barrier and have enabled the direct visualization of the dynamics of submicroscopic particles and individual molecules. On the other side of the scale, light-sheet illumination techniques allow the investigator to capture the development of an entire organism, one cell at a time. Finally, in the field of medical imaging, magnetic resonance scanning techniques have provided detailed images of the structure of the living human body and the activity of the brain.

This series of manuals originated in the Cold Spring Harbor Laboratory course on Imaging Structure and Function of the Nervous System, taught continuously since 1991. Since its inception, the course quickly became a "watering hole" for the imaging community and especially for neuroscientists and cellular and developmental neurobiologists, who are traditionally always open to microscopy approaches. The original manual, published in 2000, sprang from the course and focused solely on neuroscience, and its good reception, together with rapid advances in imaging techniques, led to a second edition of the manual in 2005. At the same time, the increased blurring between neuroscience and developmental biology made it necessary to encompass both disciplines, so the original structure of the manual was revised, and many new chapters were added. But even this second edition felt quickly dated in this exploding field. More and more techniques have been developed, requiring another update of the manual, too unwieldy now for a single volume. This is the reasoning behind this new series of manuals, which feature new editors and a significant number of new methods. The material has been split into several volumes, thus allowing a greater depth of coverage. The first book, *Imaging: A Laboratory Manual*, is a background text focused on general microscopy techniques and with some basic theoretical principles, covering techniques that are widely applicable in many fields of biology and also some specialized techniques that have the potential to greatly expand the future horizon of this field. A second manual, *Imaging in Neuroscience: A Laboratory Manual*, keeps the original focus on nervous system imaging from the Cold Spring Harbor Imaging course. A third volume, *Imaging in Developmental Biology: A Laboratory Manual*, now solely deals with developmental biology, covering imaging modalities particularly suited to follow developmental events. There are plans to expand the series into ultrastructural techniques and medical-style imaging, such as functional magnetic resonance imaging (fMRI) or positron emission tomography (PET), so more volumes will hopefully follow these initial three, which cover mostly optical-based approaches.

Like its predecessors, these manuals are not microscopy textbooks. Although the basics are covered, I refer readers interested in a comprehensive treatment of light microscopy to many of the excellent texts published in the last decades. The targeted audience of this series includes students and researchers interested in imaging in neuroscience or developmental or cell biology. Like other CSHL manuals, the aim has been to publish manuals that investigators can have and consult at their setup or bench. Thus, the general philosophy has been to keep the theory to the fundamentals and concentrate instead on passing along the little tidbits of technical knowledge that make a particular technique or an experiment work and that are normally left out of the methods sections of scientific articles.

This series of manuals has only been possible because of the work and effort of many people. First, I thank Sue Hockfield, Terri Grodzicker, Bruce Stillman, and Jim Watson, who conceived and supported the Imaging course over the years and planted the seed blossoming now in these manuals and, more importantly, in the science that has spun out of this field. In addition, the staff at CSHL Press has been exceptional in all respects, with special gratitude to John Inglis, responsible for an excellent team with broad vision, and David Crotty, who generated the ideas and enthusiasm behind this new series. Also, Inez Sialiano, Mary Cozza, Michael Zierler, Kaaren Janssen, Catriona

Simpson, Virginia Peschke, Judy Cuddihy, Martin Winer, Kevin Griffin, Kathleen Bubbeo, Lauren Heller, Susan Schaeffer, Jan Argentine, and Denise Weiss worked very hard, providing fuel to the fire to keep these books moving, and edited them with speed, precision, and intelligence. More than anyone, they are the people responsible for their timely publication. Finally, I honor the authors of the chapters in these books, many of them themselves past instructors of the CSH Imaging course and of similar imaging courses at institutions throughout the world. Teaching these courses is a selfless effort that benefits the field as a whole, and these manuals, reflecting the volunteer efforts of hundreds of researchers, who not only have taken the time to write down their technical knowledge but have agreed to generously share it with the rest of the world, are a beautiful example of such community cooperation. As Leibniz foresaw, "lens grinding" is a profession that is indeed meaningful and needs the training of young people.

— RAFAEL YUSTE

Preface to Book 1

THE PURPOSE OF THIS BOOK IS TO SERVE AS THE introduction to, and common base for, a series of laboratory manuals that cover different aspects of biological imaging. At launch, this series includes a general manual on imaging techniques, a second one on neuroscience applications, and a third one on developmental biology. This first book covers basic microscopy techniques and also some more advanced ones that have not yet become commonplace in the laboratory but that are included because of their great potential.

In organizing the material for this first manual I was aware of the difficulty inherent in splitting this dynamic field into manageable sections. The techniques discussed here span many scales and applications and are based on many different optical principles and on combinations of them. Science is fluid and the reader should be aware that the sections of the book are merely artificial placeholders to help the reader find the relevant material faster.

The book is divided into three main sections. The first (Instrumentation) focuses on the hardware and covers the basics of light microscopy, light sources, cameras, and image processing. This section also covers some novel technologies, such as liquid crystal, acousto-optical tunable filters, ultrafast lasers, and grating systems; discusses different forms of imaging, from DIC to confocal to two-photon—techniques that are becoming relatively standard in biological research institutes; and ends with a chapter that discusses the challenges of making the microscope environment compatible with the survival of common biological preparations.

The second section (Labeling and Indicators) focuses on labeling methods to stain cells, organelles, and proteins or to measure ions or molecular interactions. It includes some well-established methods, such as immunological and nonimmunological staining, and newer genetic engineering techniques where one tags a protein directly or indirectly with a fluorophore. This section also covers fluorescence and luminescent indicators of several intracellular biochemical pathways, with particular emphasis on measurements of calcium dynamics.

The third section of the manual (Advanced Microscopy) covers less established techniques, many of them at the forefront of imaging research. This section is organized by scale, covering first imaging of molecules, then imaging of cells, and then imaging of tissues or entire organisms. In addition, this section has a separate set of chapters dealing with strategies to perform fast laser imaging, an area of rapid development that aims to enhance the slow time resolution arising from the serial scanning by laser microscopes. Finally, there are three chapters on the use of caged compounds, photochemical actuators that enable the optical manipulations of cells and tissues in situ. The ability to optically alter the concentration of a substance in a small region of a cell or a tissue is turning imaging from a descriptive technique into an experimental one.

The manual ends with a series of appendices, including a glossary of imaging terms, useful information on spectra, lenses, and filters, and instructions for handling imaging hardware safely.

Besides the people and institutions already acknowledged in the series preface, a separate thanks goes to the funding agencies that have made my work as “imagist” possible over the years. The

research of my group has been supported by the generosity of the National Eye Institute, the Howard Hughes Medical Institute, and the Kavli Foundation. Columbia University, and its Department of Biological Sciences and its Neuroscience Program, has been a wonderful environment in which to work and pursue my dreams as a researcher and scholar. I would also like to thank the members of my laboratory and, in particular, Darcy Peterka, Kira Poskanzer, Roberto Araya, and Alan Woodruff, who helped me in the final copy editing of all the chapters of this and the other books in the series. In addition, I especially thank Fred Lanni and Arthur Konnerth for co-editing the first two editions of the manual and for all the wonderful late-night discussions when we ran the CSH course. Finally, as they say in Basque, *hau etxekoentzat da* (this here is for the people of the house). I dedicate this book to my *etxekoak*, my extended group of family and friends, because it is from them that I gather my strength.

— RAFAEL YUSTE

Index

Page references followed by f denote figures; page references followed by t denote tables.

C

D

E

U

6 Spinning-Disk Systems

Tony Wilson
Department of Engineering Science, University of Oxford, Oxford OX1 3PJ, United Kingdom

ABSTRACT

In this chapter, we discuss the origin of optical sectioning in optical microscopy in terms of the structure of the illumination and the structure of the detection. This parallel approach to image formation allows the introduction of high-speed light efficient approaches to obtaining optically sectioned images in real time, using conventional microscope illumination systems.

INTRODUCTION

The popularity of the confocal microscope in life science laboratories around the world is undoubtedly due to its ability to permit volume objects to be imaged and to be rendered in three dimensions. It is important to realize that the confocal microscope itself does not produce three-dimensional images. Indeed, it does the opposite. The critical property that the confocal microscope possesses, which the conventional microscope does not, is its ability to image efficiently (and in-focus) only those regions of a volume specimen that lie within a thin section in the focal region of the microscope. In other words, it is able to reject (i.e., vastly attenuate) light originating from out-of-focus regions of the specimen. To image a three-dimensional volume of a thick specimen, it is necessary to take a whole series of such thin optical sections as the specimen is moved axially through the focal region. Once this through-focus series of optically sectioned images has been recorded, it is a matter of computer processing to decide how the three-dimensional information is to be presented.

Any optical microscope that is to be used to produce three-dimensional images must have the ability to record a thin optical section. There are many methods for producing optical sections, of which the confocal optical system is just one. We shall review these methods and shall describe a number of convenient methods of implementation that can lead to, among other things, real-time image formation.

OPTICAL SECTIONING

In the following discussion, we shall restrict our attention to bright-field or (single-photon) fluorescence imaging in which the optical sectioning results from the optical system of the microscope rather

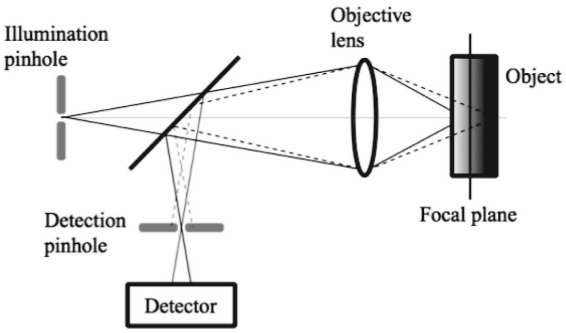

FIGURE 1. The physical origin of the depth discrimination or optical sectioning property of the confocal optical system. A barrier in the form of a pinhole aperture is used to physically prevent (block) light originating from regions in the specimen from passing through the pinhole and, hence, being detected by the photodetector and thus contributing to the final image contrast.

than by any nonlinear interaction between the probe light and the specimen. To be able to make general remarks about various optical systems, we will describe the design in terms of the structure of the illumination and in terms of the structure of the detection. To put these terms in context, we note that, in the conventional fluorescence microscope, we essentially illuminate the specimen uniformly and image the fluorescence emitted by the specimen to an image plane in which we view the image intensity either directly by eye or via a charge-coupled device (CCD) camera. In this case, the structure of the illumination is uniform as is the structure of the detection, and the microscope does not show optical sectioning. In the confocal microscope, on the other hand, we use point illumination and point detection to introduce optical sectioning. The optical principle can be seen in Figure 1, where we see that the action of the point detector is to block light that originates in out-of-focus regions from passing through the pinhole (Wilson and Sheppard 1984; Wilson 1990). Its efficacy in achieving this, which also determines the axial width of the optical section, clearly depends on the size and the shape of the pinhole used. An infinitely large pinhole, for example, would block no light and, hence, provide no optical sectioning. This effect is discussed in detail elsewhere (Wilson 1989, 1995; Wilson and Carlini 1987). The system illustrated in Figure 1 might be regarded as the ultimate in structured illumination and detection—point illumination and point detection—and has resulted in the desired optical sectioning but has only produced an image of a single point of the specimen. To produce an image of a finite region of the specimen, it is necessary to introduce scanning so as to probe the entire specimen. In general terms, we have introduced a particular structure to both the illumination and the detection, which we might also refer to as modulation, such that that the optical system shows optical sectioning. We must then remove any undesirable side effects of this modulation to obtain the desired image. In this particular case, the modulation results in a restriction of the field of view to a single point; hence, a demodulation stage consisting of scanning is required to restore the field of view. We shall return to practical implementations of the demodulation below, but we note that there are two basic approaches. In the first, a single point source–point detector confocal system is used together with a scanning mechanism designed to scan a single focused spot of light with respect to the specimen. In the second approach, a number of confocal systems is constructed in parallel. These serve to produce many focused spots of light, which are used to image different parts of the specimen simultaneously. This is achieved by using an aperture disk consisting of many pinholes.

Another way to think about optical sectioning is in terms of the way in which the spatial frequencies present in the specimen are imaged. In essence, we describe the fluorescence distribution within the specimen in terms of its spatial frequency spectrum (Fourier content) and ask how each of these spatial frequency components is imaged by the optical system. The optical transfer function of the optical system provides the answer to this question because it describes how efficiently each spatial frequency is imaged. A requirement that the system show optical sectioning might be that the contrast of all spatial frequencies must attenuate as the microscope is defocused. Figure 2A shows

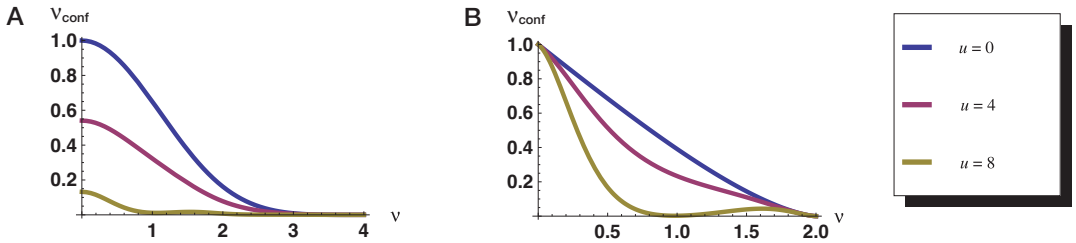

FIGURE 2. (*A*) The confocal optical transfer function as a function of the normalized spatial frequency for a number of values of defocus *u*. The normalized defocus *u* is related to the actual defocus *z* by $u = 4knz \sin^2(\alpha/2)$ in which the numerical aperture (NA) is given by NA = $n \sin(\alpha)$. The normalized spatial frequency ν is related to the actual spatial frequency *f* measured in the focal plane via $\nu = f\lambda/\text{NA}$. We note that all spatial frequencies attenuate with increasing defocus. (*B*) The optical transfer function of the conventional microscope as a function of the normalized spatial frequency for a number of values of defocus *u*. Note that all spatial frequencies attenuate with increasing defocus apart from the zero spatial frequency case.

the optical transfer function of a confocal fluorescence microscope, in which we see that the contrast of all spatial frequencies attenuates with increasing defocus. Figure 2B, on the other hand, shows the equivalent function for the conventional fluorescence microscope. In this case, we see that it is only the zero spatial frequency whose contrast does not attenuate with increasing defocus. The contrast of all other spatial frequencies is seen to reduce as the degree of defocus increases.

Although the aperture disk consisting of many pinholes was described above as a natural way to parallelize many confocal microscopes, it may also be thought of as acting like a mask that causes the whole specimen to be illuminated by a particular structure. It is natural, therefore, to ask whether there are other simple forms of structure to the illumination that may be used to introduce optical sectioning. If we modify the illumination system of the microscope so as to project a single spatial frequency grid pattern onto the object, the microscope will then image efficiently only that portion of the object where the grid pattern is in focus (Fig. 2B). We will thus obtain an optically sectioned image of the object but with the (unwanted) grid pattern superimposed. The rate of attenuation with defocus or optical sectioning strength will, of course, depend on the particular spatial frequency that is projected onto the object (Fig. 2B). For example, a 40-μm pitch grid imaged using a 63x, 1.4-NA objective lens with light of wavelength 0.5 μm yields ν = 0.56, whereas an 80-μm pitch grid yields ν = 0.28 and a 20-μm pitch grid gives ν = 1.12. Here we have used the structure of the illumination (harmonic modulation) to introduce optical sectioning. The price is that the optical section is now delineated or labeled by that portion of the image where the superimposed grid pattern is visible. It is now necessary to introduce a demodulation stage whereby the out-of-focus regions as well as the grid pattern are removed from the "raw" image to reveal the desired optically sectioned image. This may be done in two ways, computationally or optically. The computational approach typically requires that three raw images be taken, corresponding to three different spatial positions of the illumination grid. This is the approach taken in several commercial structured illumination systems such as the OptiGrid system from Qioptiq (Neil et al. 1997). The alternative optical demodulation technique, which will be discussed in this chapter, is to combine harmonic structured illumination with harmonic structured detection. In this case an identical mask is used for both the illumination and detection. Demodulation is carried out by scanning the masks in synchronism.

We conclude this section by noting that a system with uniform structure of illumination and detection—the conventional microscope—does not exhibit optical sectioning, whereas one with point illumination and point detection—the confocal system—does exhibit optical sectioning. An equivalent way of saying this is to say that the conventional system employs zero spatial frequency illumination and detection whereas the point source/detector confocal system employs full spatial frequency illumination and detection. The harmonic approach we have just discussed, on the other hand, lies somewhere between these approaches, because only one spatial frequency is used for both the illumination and detection. The nature of the illumination/detection used in the last two cases requires that a further demodulation step—often achieved by scanning—be performed to provide a full field optically sectioned image.

PRACTICAL REALIZATION OF OPTICAL SECTIONING MICROSCOPES

We shall now discuss the practical implementation of these two approaches to achieve optical sectioning. We begin with the traditional confocal system.

It is clear from the previous discussion that an optical system consisting of a single point source and single point detector serves to discriminate against light originating from out-of-focus planes. Figure 1 shows the generic optical system. The light source is typically a laser, because traditional microscope illumination systems are insufficiently bright. A photomultiplier tube has usually been used as the photodetector. Because this system probes only one point of the specimen, scanning must be used to obtain an image of a whole optical section. This may be achieved in a variety of ways. The specimen may be physically scanned with respect to the fixed focal spot. Alternatively the objective lens may also be scanned. These approaches have advantages from both the optical performance and optical design points of view but are generally considered to be impractical. In most commercial designs, therefore, the specimen is fixed and the scanning is achieved by scanning the focused spot of light across the fixed specimen by the use of galvonometer mirror scanners. This allows an optical section to be easily recorded. To record the next optical section, however, it is necessary to physically move the specimen axially to bring the next region into the focal volume of the confocal microscope. Commercial systems do not allow this important z-scanning step to be performed quickly, so this represents a bottleneck in the speed with which a through-focus set of images may be obtained. Recent work has shown that high-speed optical refocusing can be achieved, and hence this bottleneck may be removed (Botcherby et al. 2007). Although the layout of Figure 1 is typical, there are problems to be overcome relating to system alignment in the sense that the detector pinhole must be located in a position optically equivalent to the source pinhole. These problems may be resolved if a reciprocal geometry is employed in which the same pinhole is used both as source and detector pinhole. In practice these systems are often more easily implemented when a single-mode optical fiber replaces the pinhole (Wilson and Kimura 1991). However, all of these approaches involve the use of one confocal optical system, and the image is obtained serially by the appropriate scanning of the spot in three dimensions with respect to the specimen.

An advantage may be gained by building an optical layout consisting of many confocal systems lying side by side. In this way many parts of the specimen will be imaged confocally at the same time. This has the advantage of increasing image acquisition speed as well as dispensing with the need to use laser illumination. Each pinhole acts as both the illumination and detection pinhole and so the system acts rather like a large number of parallel, reciprocal geometry, confocal microscopes, each imaging a specific point on the object. However, we need to remember that the confocal system achieves depth discrimination by blocking out-of-focus light reaching the image by the use of a limiting pinhole detector. This observation leads us to conclude that the neighboring confocal systems must be placed sufficiently far apart that any out-of-focus light from one confocal system is not collected by an adjacent system. In other words, we must prevent cross talk between neighboring confocal systems. In practice this means that the pinholes must be placed on the order of 10 times their diameters apart, which has two immediate consequences. First, only a small amount—typically 1%—of the available light is used for imaging, and, second, the wide spacing of the pinholes means that the object is only sparsely probed. To probe—and hence image—the whole object, it is usual to arrange the pinhole apertures in a series of Archimedean spirals and to rotate the (Nipkow) disk. The generic layout of any system that is designed to contain many confocal systems operating in parallel is shown in Figure 3A. The original idea for such an approach goes back to Mojmir Petrán in the late 1960s (Petrán et al. 1968). A single-sided variant was subsequently introduced by Kino and his colleagues (Xiao and Kino 1987). The key element to these systems is a spinning Nipkow disk containing many pinholes. These systems are capable of producing high-quality images without the need to use laser illumination in real time at both television rate and higher imaging speeds. A further development, which does, however, require the use of laser illumination and, hence, restricts the use to fluorescence imaging, is to introduce an array of microlenses to concentrate the illumination laser light into the source pinholes (Ichihara et al. 1996).

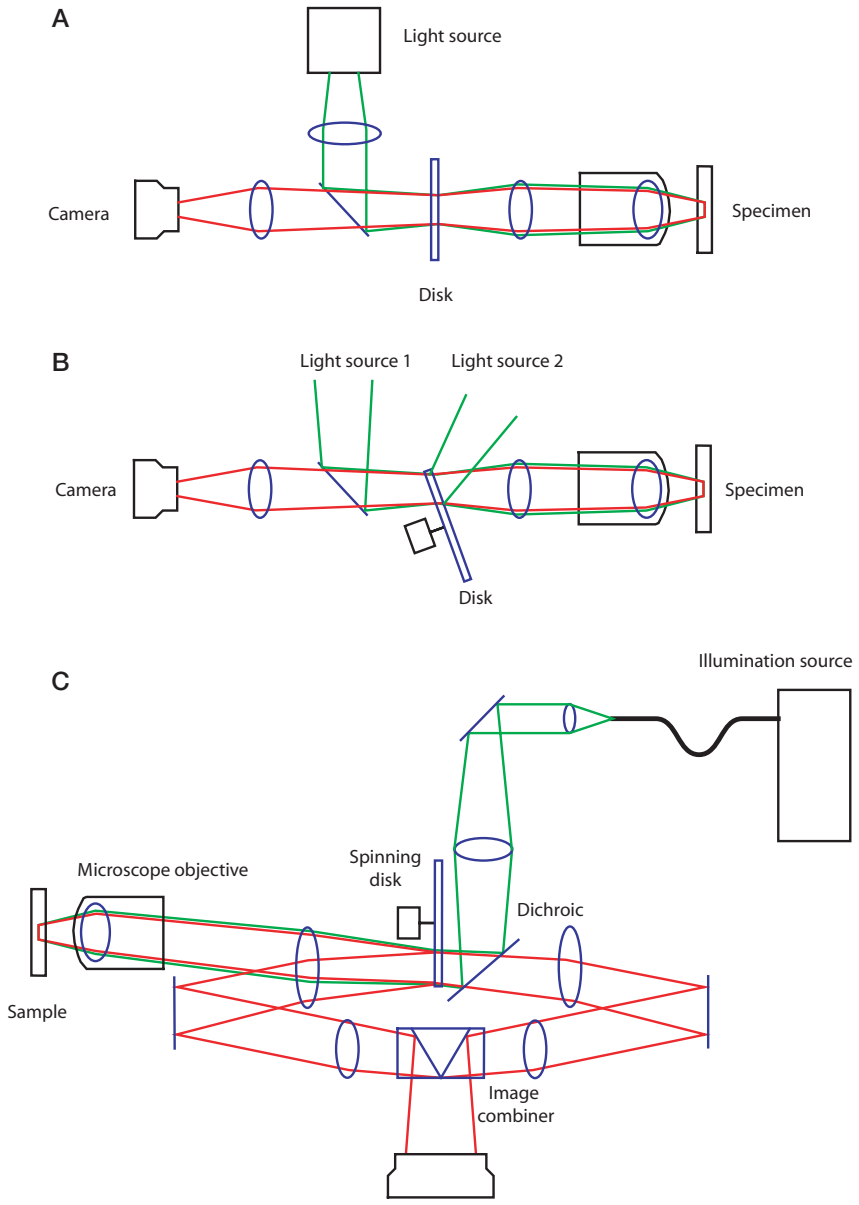

FIGURE 3. (*A*) The generic form of a spinning-disk-based microscope system. In the case of the tandem-scanning microscope, the disk consists of a large number of pinholes, each of which acts as a reciprocal geometry confocal system. The pinholes, which are placed far apart to prevent cross talk between adjacent confocal systems, are usually arranged in an Archimedean spiral on a Nipkow disk. Rotation of the disk causes the entire specimen to be imaged. In the case of the correlation code microscope, the appropriate codes are impressed photolithographically onto the disk, which is then rotated to effect the desired time-dependent correlation codes. In the harmonic illumination and detection case, a stripe pattern is imposed on the disk. In this case, the disk is spun to achieve the desired demodulation. (*B*) An example of a double-sided operation in which two light sources are used to sequentially generate the two composite images: conventional plus confocal and conventional minus confocal. (*C*) An optical configuration that permits both composite images to be recorded simultaneously, thereby removing any motion artifacts.

One approach to make greater use of the available light is to place the pinholes closer together. However, this means that cross talk between the neighboring confocal systems inevitably occurs; hence, a method must be devised to prevent this. To achieve this goal, the Nipkow disk of the tandem-scanning microscope is replaced with an aperture mask consisting of many pinholes placed as close together as possible. This aperture mask has the property that any of its pinholes can be opened and closed independently of the others in any desired time sequence. This might be achieved, for

example, by using a liquid-crystal spatial light modulator. Because we require there to be no cross talk between the many parallel confocal systems, it is necessary to use a sequence of openings and closings of each pinhole that is completely uncorrelated with the openings and the closings of all the other pinholes. There are many such orthonormal sequences available. However, they all require the use of both positive and negative numbers, and, unfortunately, we cannot have a negative intensity of light! The pinhole is either open, which corresponds to 1, or closed, which corresponds to 0. There is no position that can correspond to –1. The way to avoid the dilemma is to obtain the confocal signal indirectly. To use a particular orthonormal sequence $b_i(t)$ of plus and minus 1s, for the ith pinhole, we must add a constant offset to the desired sequence to make a sequence of positive numbers, which can be encoded in terms of pinhole opening and closing. Thus, we encode each of the pinhole openings and closings as $(1 + b_i(t))/2$, which will correspond to open (1) when $b_i(t) = 1$ and to close (0) when $b_i(t) = -1$. The effect of adding the constant offset to the desired sequence is to produce a composite image that will be partly confocal because of the $b_i(t)$ terms and partly conventional because of the constant term. The method of operation is now clear. We first take an image with the pinholes encoded as we have just discussed and so obtain a composite conventional plus confocal image. We then switch all the pinholes to the open state to obtain a conventional image. It is then a simple matter to subtract the two images in real time using a computer to produce the confocal image.

Although this approach may be implemented using a liquid-crystal spatial light modulator, it is cheaper and simpler merely to impress the correlation codes photolithographically on a disk and to rotate the disk so that the transmissivity at any picture point varies according to the desired orthonormal sequence. A blank sector may be used to provide the conventional image. If this approach is adopted, then all that is required is to replace the single-sided Nipkow disk of the tandem-scanning microscope with a suitably encoded aperture disk (Juskaitis et al. 1996a,b). We note that the coded sector on the disk may be coded so as to provide the appropriate correlation codes, or, alternatively, it may consist of a pattern of grid lines to simulate the harmonic illumination/detection case (Neil et al. 1998).

Double-Sided Operation

We have seen that the image obtained from the coded sector of the disk is a composite image from which the conventional image needs to be removed. If, rather than use a blank sector, we were to encode the whole disk such that the image we obtained may be written as $I_1 = I_{conv} + I_{conf}$, we would need to find another way to remove the conventional image. One approach is suggested in Figure 3B in which a second light source is used. In this case, a composite image of the form $I_2 = I_{conv} - I_{conf}$ is obtained. It is clear that a confocal image $I_1 - I_2 = 2I_{conf}$ may be readily extracted with a more efficient use of light than in the single-sided disk case in which I_1 and I_{conv} are obtained sequentially.

Although such an approach is entirely feasible, it does require extremely careful design so as to provide equivalent uniform illumination at each flip of the mirror. A preferred approach might be to use a single light source and a single camera. The optical system (Fig. 3C) would be such that the camera recorded the two required images simultaneously, thus eliminating any possibility of motion and other artifacts between the capture of the two required raw images. We note that these systems operate well with standard microscope illuminators (e.g., Exfo Inc.) and standard CCD cameras, producing images that are directly comparable to those taken with traditional laser-based confocal systems. Figure 4 shows a typical through-focus series of images together with a standard three-dimensional rendering.

CONCLUSION

The confocal microscope is now firmly established as a workhorse instrument in laboratories throughout the world because of its ability to enable volume specimens to be imaged in three dimensions. However, there is still much work to be performed to make these instruments suitable for high-speed

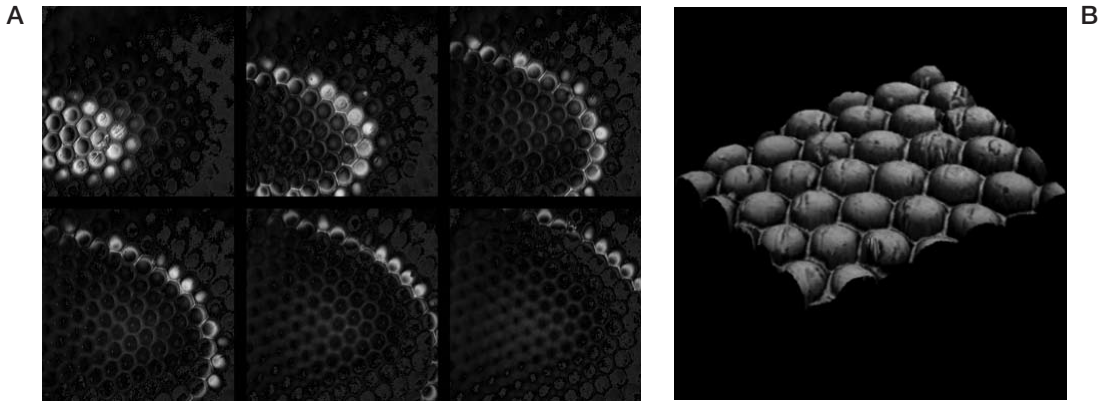

FIGURE 4. (*A*) A through-focus series of images taken of the eye of a fly. (*B*) A three-dimensional rendering of the eye of the fly constructed from the through-focus series of images presented in *A*.

imaging of living specimens. Further advances will require a combination of new contrast mechanisms together with advances in instrument design. This chapter has described a parallelization of the traditional confocal principle so as to permit real-time confocal imaging without the need for laser illumination. The concept of structured illumination and structured detection has been introduced to stimulate the search for alternative methods of image encoding to reveal optical sectioning.

REFERENCES

Botcherby EJ, Juskaitis R, Wilson T. 2007. Real-time scanning microscopy in the meridional plane. *Opt Express* **34:** 1504–1506.

Botcherby EJ, Juskaitis R, Wilson T. 2009. Real-time extended depth of field microscopy. *Opt Express* **16:** 21843–21848.

Ichihara A, Tanaami T, Isozaki K, Sugiyama Y, Kosugi Y, Mikuriya K, Abe M, Uemura I. 1996. High-speed confocal fluorescence microscopy using a Nipkow scanner with microlenses for 3-D imaging of single fluorescent molecule in real-time. *Bioimages* **4:** 57–62.

Juskaitis R, Neil MAA, Wilson T, Kozubek M. 1996a. Efficient real-time confocal microscopy with white light sources. *Nature* **383:** 804–806.

Juskaitis R, Neil MAA, Wilson T, Kozubek M. 1996b. Confocal microscopy by aperture correlation. *Opt Lett* **21:** 1879–1881.

Neil MAA, Juskaitis R, Wilson T. 1997. Method of obtaining optical sectioning using structured light in a conventional microscope. *Opt Lett* **22:** 1905–1907.

Neil MAA, Wilson T, Juskaitis R. 1998. A light efficient optically sectioning microscope. *J Microsc* **189:** 114–117.

Petrán M, Hadravsky M, Egger M, Galambos R. 1968. Tandem scanning reflected light microscope. *J Opt Soc Am* **58:** 661–664.

Wilson T. 1989. Optical sectioning in confocal fluorescent microscopes. *J Microsc* **154:** 143–156.

Wilson T. 1990. *Confocal microscopy*. Academic, London.

Wilson T. 1995. The role of the pinhole in confocal imaging system. In *Handbook of biological confocal microscopy*, 2nd ed. (ed. Pawley JB), pp. 167–182. Plenum, New York.

Wilson T, Carlini AR. 1987. Size of the detector in confocal imaging systems. *Opt Lett* **12:** 227–229.

Wilson T, Kimura S. 1991. Confocal scanning optical microscopy using a single mode fiber for signal detection. *Appl Opt* **30:** 2143– 2150.

Wilson T, Sheppard CJR. 1984. *Theory and practice of scanning optical microscopy*. Academic, London.

Xiao GQ, Kino GS. 1987. A real-time scanning optical microscope. *Proc SPIE* **809:** 107–113.

45 Array Tomography
High-Resolution Three-Dimensional Immunofluorescence

Kristina D. Micheva, Nancy O'Rourke, Brad Busse, and Stephen J Smith
Department of Molecular and Cellular Physiology, Stanford University School of Medicine, Stanford, California 94305

ABSTRACT

Array tomography is a volumetric microscopy method based on physical serial sectioning. Ultrathin sections of a plastic-embedded tissue specimen are cut using an ultramicrotome, bonded in ordered array to a glass coverslip, stained as desired, and then imaged. The resulting two-dimensional image tiles can then be computationally reconstructed into three-dimensional volume images for visualization and quantitative analysis. The minimal thickness of individual sections provides for high-quality, rapid staining and imaging, whereas the array format provides for reliable and convenient section handling, staining, and automated imaging. In addition, the array's physical stability permits the acquisition and registration of images from repeated cycles of staining, imaging, and stain elution and from imaging by multiple modalities (e.g., fluorescence and electron microscopy). Array tomography offers high resolution, depth invariance, and molecular discrimination, which justify the relatively difficult tomography array fabrication procedures. With array tomography it is possible to visualize and quantify previously inaccessible features of tissue structure and molecular architecture. This chapter will describe one simple implementation of fluorescence array tomography and provide protocols for array tomography specimen preparation, image acquisition, and image reconstruction.

INTRODUCTION

Our understanding of tissue function is constrained by incomplete knowledge of tissue structure and molecular architecture. Genetics, physiology, and cell biology make it overwhelmingly clear that all cell and tissue function depends critically on the composition and precise three-dimensional configuration of subcellular organelles and supramolecular complexes, and that such structures may consist of very large numbers of distinct molecular species. Unfortunately, the intricacies of tissue molecular architecture badly outstrip the analytical capability of all presently known tissue imaging methods.

Array tomography is a new high-resolution, three-dimensional microscopy method based on constructing and imaging two-dimensional arrays of ultrathin (70–200 nm thickness) specimen sections on solid substrates. (The word "tomography" derives from the Greek words *tomos*, to cut or section, and *graphein*, to write: The moniker "array tomography" thus simply connotes the "writing" of a volume image from an array of slices.) Array tomography allows immunofluorescence imaging of tissue samples with resolution, quantitative reliability, and antibody multiplexing capacity that is greatly superior to previous tissue immunofluorescence methods (Micheva and Smith 2007). Array tomography was developed with neuroscience applications in mind (e.g., Smith 2007; Stephens et al. 2007; Koffie et al. 2009), and the following description will be illustrated with examples from neuroscience and particularly from studies of synapses and circuits in rodent brain.

ARRAY TOMOGRAPHY PROCEDURES

A sequence of eight steps for a very basic array tomography protocol is illustrated in Figure 1. Array tomography begins with (Step 1) the chemical fixation of the specimen, followed by (Step 2) dissection and embedding in resin (LR White). Resin-embedded specimen blocks are then (Step 3) mounted in an ultramicrotome chuck, trimmed, and prepared for ultrathin sectioning. Block preparation includes careful trimming of the block edges and application of a tacky adhesive to the top and bottom block edges. As shown in the magnified detail of Step 3, this adhesive causes the spontaneous formation of a stable splice between successive serial sections as they are cut by the ultramicrotome's diamond knife blade. The automated cycling of a standard ultramicrotome produces automatically a ribbon up to 45 mm in length, which may consist of more than 100 serial sections held on a water surface. Ribbons are then manually transferred to the surface of a specially coated glass coverslip (Step 4). The resulting array can be stained using antibodies or any other desired reagents (Step 5). After immunostaining, arrays can be imaged using fluorescence microscopy (Step 6). The minimal thickness of array sections promotes very rapid and excellent staining and imaging, whereas the array format promotes convenient and reliable handling of large numbers of serial sections. The individual two-dimensional section images are then computationally stitched and aligned into volumetric image stacks (Step 7) to provide for three-dimensional image visualization and analysis (Fig. 2). The volumetric image stacks are stored electronically for analysis and archiving

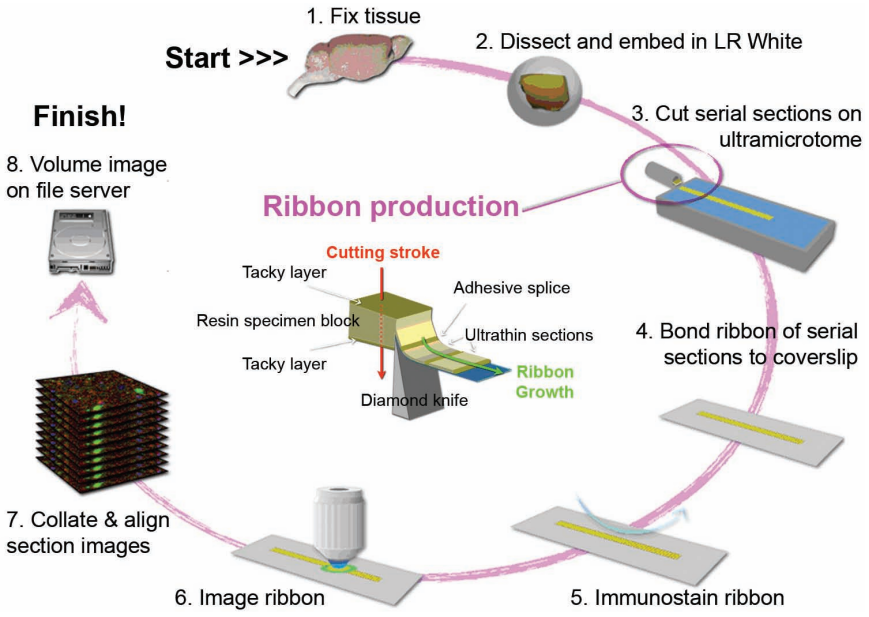

FIGURE 1. The sequence of steps for a basic immunofluorescence array tomography process.

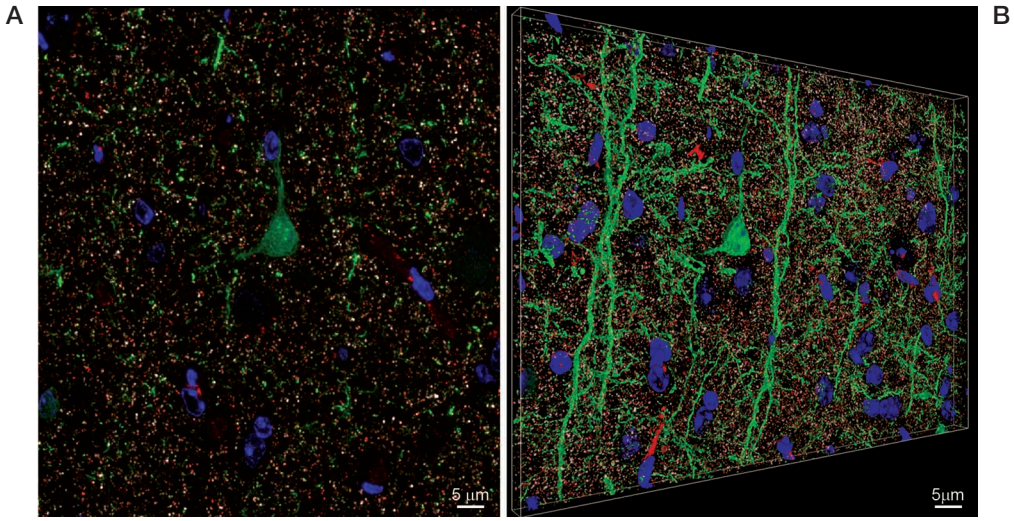

FIGURE 2. Array tomographic images of layer 5 neuropil, barrel cortex of YFP-H Thy-1 transgenic mouse (Feng et al. 2000). Yellow fluorescent protein (YFP) expression in a subset of pyramidal cells (green), Synapsin 1 immunostaining (white), PSD95 (red), DAPI staining of nuclear DNA (blue). (*A*) Four-color fluorescence image of a single, ultrathin section (200 nm). (*B*) Volume rendering of a stack of 30 sections after computational alignment as described in this chapter.

(Step 8). Although array tomography procedures are at present relatively complex and demanding in comparison to many other imaging methods, each of the steps lends itself potentially to automated and highly parallel implementations, and for many applications the advantages outlined below can easily justify this extra effort.

Resolution

The volumetric resolution of fluorescence array tomography compares very favorably with the best optical sectioning microscopy methods. The axial resolution limit for array tomography is simply the physical section thickness (typically 70 nm). For a confocal microscope, the *z*-axis resolution is limited by diffraction to ~700 nm. The confocal's limiting *z*-axis resolution is usually worsened, however, by spherical aberration when a high-numerical-aperture (high-NA) objective is focused more deeply than a few micrometers into any tissue specimen. Array tomography physical sectioning thus improves on ideal confocal optical sectioning by at least an order of magnitude. Spherical aberrations also adversely impact the lateral resolution of confocal microscopes as they are focused into a tissue depth. Array tomography avoids this problem, because the high-NA objective is always used at its design condition (immediate contact between specimen and coverslip), with no chance of focus depth aberration. The degradation of lateral resolution that occurs at focus depths of just a few micrometers can easily exceed a factor of 2 (see http://www.microscopy.fsu.edu/), so a very conservative approximation would imply that array tomography using ordinary high-NA, diffraction-limited optics would improve volumetric resolution (the product of improvements in *x*-, *y*-, and *z*-axes) by a factor of 40 (= 2 × 2 × 10). The improved volumetric resolution realized by array tomography can be very significant. For instance, individual synapses in situ within mammalian cortex generally cannot be resolved optically from their nearest neighbors by confocal microscopy but can be resolved quite reliably by array tomography (Micheva and Smith 2007).

Depth Invariance

The major limitation to quantitative interpretation of whole-mount tissue immunofluorescence images arises from reductions in both immunostaining and imaging efficiencies as focal plane depth increases. Diffusion and binding regimes typically limit the penetration of labeling antibodies to the

first few micrometers below the surface of a tissue, even after multiday incubations. Imaging efficiency likewise decreases with depth, as increasing spherical aberration and light scattering reduce signals profoundly with focal plane depths of just a few micrometers. These staining and imaging efficiency gradients make any quantitative comparison of specimen features at different depths with whole-mount (e.g., confocal) volume microscopy difficult and unreliable. Array tomography completely circumvents depth dependence issues, because each specimen volume element is stained identically owing to minimal section thickness, and imaged identically because every section is bonded directly to the coverslip surface.

Multiplexity

Traditional multicolor immunofluorescence techniques have provided compelling evidence for the localization of multiple molecular species at individual subcellular complexes. For example, because there is a very large number and a great diversity of distinct molecules at individual synapses, there is a pressing need for imaging techniques that can simultaneously discriminate many more than the three or four species that can be distinguished by standard multicolor immunofluorescence. Attempts have been made in the past to improve the multiplexity of immunofluorescence microscopy by repeated cycles of staining, imaging, and stain elution, but the results have been disappointing owing to the tendency of antibody elution treatments to destroy samples. In array tomography, specimens are stabilized by the embedding resin matrix and by tight attachment to the coverslip substrate. An example of multiplexed staining with array tomography is shown in Figure 3. We have shown as many as nine cycles of staining, imaging, and elution thus far (Micheva and Smith 2007). With four fluorescence "colors" per cycle, this would mean that 36 or more antigens could be probed in one specimen. We now routinely acquire four colors in each of three cycles for a total of 12 marker channels. Although 12–36 markers may still fall short of the degree of multiplexing needed to fully probe the many and diverse molecules composing a synapse, it is a substantial advance in comparison to traditional multicolor immunofluorescence methods.

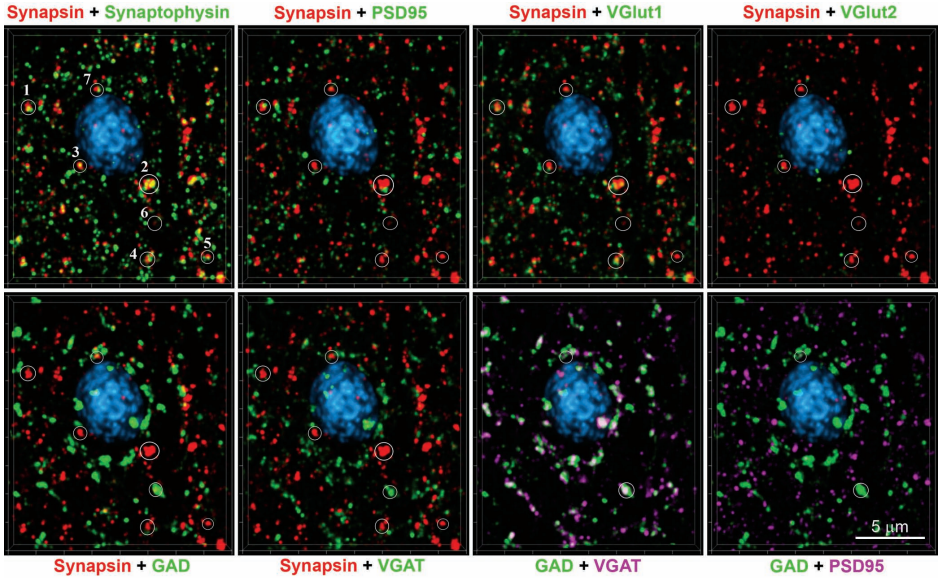

FIGURE 3. Multiplexed staining for seven synaptic proteins in mouse cerebral cortex (layer 2/3, barrel cortex) using five cycles of staining and elution. This volume of 18 x 16 x 1.3 µm was reconstructed from 19 serial sections (70 nm each). Individual synapsin puncta 1, 2, and 3 colocalize with synaptophysin and VGlut1 and are closely apposed to PSD95 and thus appear to be excitatory synapses. Synapsin puncta 4–7 colocalize with synaptophysin, but do not have adjacent PSD95 puncta. Puncta 6 and 7 also colocalize with GAD and VGAT and thus have the characteristics of inhibitory synapses.

Volume Field of View

In principle, array tomography offers unique potential for the acquisition of high-resolution volume images that extend "seamlessly" over very large tissue volumes. The depth invariance of array tomography noted above eliminates any fundamental limit to imaging in depth, whereas the availability of excellent automated image mosaic acquisition, alignment, and stitching algorithms allows tiling over arbitrarily large array areas. Ultimate limits to the continuous arrayable volume will be imposed by difficulties in tissue fixation, processing, and embedding (owing to diffusion limitations) as thicker volumes are encountered, and by mechanical issues of ultramicrotome and diamond knife engineering as block face dimensions increase. Successful array tomography has already been shown for volumes with millimeter minimum dimensions, and it seems likely that volumes with minimum dimensions of several millimeters (e.g., an entire mouse brain) may be manageable eventually.

In practice, the size of seamless array tomography volumes is limited by the requirement that numerous steps in the fabrication, staining, and imaging of arrays be performed through many iterations without failure. At present, the most error-prone steps are those involved in array fabrication, whereas the most time-consuming are those involved in image acquisition. Ongoing engineering of array fabrication materials and processes will advance present limits to the error-free production of large arrays, whereas image acquisition times will be readily reducible by dividing large arrays across multiple substrates and imaging those subarrays on multiple microscopes.

The following protocols describe one simple implementation of immunofluorescence array tomography suitable for any laboratory with standard equipment and some expertise in basic fluorescence microscopy and ultrathin sectioning. In addition, algorithms designed to fully automate the acquisition of array images are described for the benefit of any laboratory having or planning to acquire the appropriate automated fluorescence microscopy hardware and software.

Protocol A

Rodent Brain Tissue Fixation and Embedding

Careful preparation of the tissue is essential for successful array tomography. These steps take time to complete and require some practice to perfect.

MATERIALS

CAUTION: See Appendix 6 for proper handling of materials marked with <!>.
See the end of the chapter for recipes for reagents marked with <R>.

Reagents

Ethanol <!>, 4°C
Fixative <R>
Isoflurane <!> (VWR International)
LR White resin <!> (medium grade, SPI Supplies 2646 or Electron Microscopy Sciences 14381)
Mice
Wash buffer <R>, 4°C

Equipment

Capsule mold (Electron Microscopy Sciences 70160)
Dissection instruments: handling forceps, small scissors, bone rongeur, forceps #5, small spatula, scalpel
Gelatin capsules, size 00 (Electron Microscopy Sciences 70100)
Guillotine
Microscope, dissection
Microwave tissue processor system (PELCO with a ColdSpot set at 12°C; Ted Pella, Inc.) (optional)
Oven (set at 51°–53°C)
Paintbrush, fine
Petri dishes, 35-mm
Scintillation vials, glass, 20-mL

EXPERIMENTAL METHOD

Dissecting and Fixing Tissue

1. Anesthetize the rodent with isoflurane.
2. Remove head using the guillotine.
3. In a hood, using the dissection tools quickly remove the brain and plunge it into a 35-mm Petri dish filled with fixative (room temperature). Remove the tissue region of interest.
4. Transfer tissue to a scintillation vial with fixative solution. Use ~1 mL of fixative per vial, or just enough to cover the tissue; excessive liquid volume will cause overheating in the microwave.

5. Microwave the tissue in the fixative using a cycle of 1 min on/1 min off/1 min on at 100–150 W. After this and each subsequent cycle feel the glass vial to check for overheating. If solutions are getting too warm (>37°C), decrease the amount of liquid added.
6. Microwave using a cycle of 20 sec on/20 sec off/20 sec on at 350–400 W. Repeat three times.
7. Leave the tissue at room temperature for ~1 h.

   If a microwave is unavailable, fix the samples at room temperature for up to 3 h or overnight at 4°C. Tissue can also be fixed by perfusion.
8. Prepare ethanol dilutions: 50%, 70%, 95%, and 100% in ultrapure H_2O. Keep at 4°C.
9. Wash the tissue in wash buffer (4°C) twice for 5 min each.
10. Transfer the tissue to a 100-mm Petri dish, cover with wash buffer, and under a dissecting microscope dissect the tissue into smaller pieces (<1 mm in at least one dimension).
11. Return the samples to scintillation vials and rinse them twice with wash buffer for 15 min each at 4°C.
12. Change to 50% ethanol (4°C) and microwave the samples for 30 sec at 350 W. Use just enough liquid to cover the tissue; excessive liquid volume will cause overheating.

    If a microwave processor is unavailable, Steps 12–20 can be performed for 5 min per step on the bench.
13. Change to 70% ethanol (4°C) and microwave the samples for 30 sec at 350 W.

Processing Samples that Contain Fluorescent Proteins

If processing samples with fluorescent proteins, then complete Steps 14–16. If samples do not contain fluorescent proteins, then skip Steps 14–16, and instead continue with Step 17.

14. Change one more time to 70% ethanol and microwave for 30 sec at 350 W.
15. Change to a mixture of 70% ethanol and LR White (1:3; if it turns cloudy add 1–2 extra drops of LR White) and microwave for 30 sec at 350 W.
16. Go to Step 20.

Processing Samples that *Do Not* Contain Fluorescent Proteins

17. Change to 95% ethanol (4°C) and microwave for 30 sec at 350 W.
18. Change to 100% ethanol (4°C) and microwave for 30 sec at 350 W. Repeat once.
19. Change to 100% ethanol and LR White resin (1:1 mixture, 4°C) and microwave for 30 sec at 350 W.

Embedding Brain Tissue

20. Change to 100% LR White (4°C) for 30 sec at 350 W. Repeat two more times.
21. Change to fresh LR White (4°C) and leave either overnight at 4°C or 3 h at room temperature.
22. Using a fine paintbrush, place the tissue pieces at the bottom of gelatin capsules (paper labels can also be added inside the capsule) and fill to the rim with LR White.

    See *Troubleshooting*.
23. Close the capsules well and put in the capsule mold.

    Gelatin capsules are used because they exclude air that inhibits LR White polymerization. The little bubble of air that will remain at the top of the capsule will not interfere with the polymerization.
24. Put the mold with capsules in the oven set at 51°–53°C. Leave overnight (~18–24 h).

TROUBLESHOOTING

Problem (Step 22): It is difficult to orient the tissue.

Solution: If tissue orientation is important, it should be dissected in a shape that will make it naturally sink in the resin the desired way—for example, for mouse cerebral cortex, a 300-μm coronal slice can be cut and trimmed to a rectangle, ~1 × 2 mm, that includes all of the cortical layers. Alternately, if the tissue is elongated and has to be cut perpendicular to the long axis, the capsules can be positioned on the side, instead of standing up in the mold.

Protocol B

Production of Arrays

Once the tissue has been embedded, the arrays are prepared. This protocol requires familiarity with ultramicrotome sectioning for electron microscopy.

MATERIALS

CAUTION: See Appendix 6 for proper handling of materials marked with <!>.
See the end of the chapter for recipes for reagents marked with <R>.

Reagents

Borax
Contact cement (DAP Weldwood)
Subbing solution <R>
Tissue, fixed and embedded as in Protocol A
Toluidine blue
Xylene <!>

Equipment

Coverslips (for routine staining: VWR International Micro Cover Glasses, 24 x 60-mm, No.1.5, 48393-252; for quantitative comparison between different arrays: Bioscience Tools High Precision Glass Coverslips CSHP-No1.5-24 x 60)
Diamond knife (Cryotrim 45; Diatome) (optional)
Diamond knife (Histo Jumbo; Diatome)
Eyelash tool
Marker
Razor blades
Paintbrush, fine
Slide warmer set at 60°C
Staining rack (Pacific Southwest Lab Equipment, Inc. 37-4470 and 4456)
Syringe
Transfer pipettes, extra fine-tip polyethylene (Fisher Scientific 13-711-31)
Ultramicrotome (e.g., Leica EM UC6)

EXPERIMENTAL METHOD

1. Prepare subbed coverslips. They can be prepared in advance and stored in coverslip boxes until needed.
   i. Put clean coverslips into the staining rack.
   ii. Immerse the rack in the subbing solution and remove bubbles formed at the surface of the coverslips using a transfer pipette.

iii. After 30–60 sec, lift out and drain off excess liquid. Leave the coverslips in a dust-free place until they are dry.

2. Using a razor blade, trim the block around the tissue. A blockface ~2 mm wide and 0.5–1 mm high works best.
3. Using a glass knife or an old diamond knife cut semithin sections until you reach the tissue. Mount a couple of the semithin sections on a glass slide and stain with 1% toluidine blue in 0.5% borax. View the stained sections under a microscope to determine whether they contain the region of interest and decide how to trim the block.
4. Trim the block again, to ensure that the blockface is not too big and the leading and trailing edges of the blockface are parallel. The Cryotrim 45 diamond knife works well for this purpose.
5. Using a paintbrush, apply contact cement diluted with xylene (1:2) to the leading and trailing sides of the block pyramid. Blot the extra glue using a tissue.
6. Insert a subbed coverslip into the knife boat of the Histo Jumbo diamond knife. You may need to push it down and wet it using the eyelash tool. Make sure that the knife angle is set at 0°.
7. Carefully align the block face with the edge of the diamond knife. If the block starts cutting at an angle, the leading and trailing edge of the block face will no longer be parallel.
8. Start cutting ribbons of serial sections (70–200 nm) with the diamond knife. In general, thinner sections stick better to the glass.

   See *Troubleshooting*.
9. When the desired length of the ribbon is achieved, carefully detach it from the edge of the knife by running an eyelash along the outer edge of the knife. Then use the eyelash to gently push the ribbon toward the coverslip, so that the edge of the ribbon touches the coverslip at the interface of the glass and the water. The edge of the ribbon will stick to the glass.
10. Using a syringe, slowly lower the water level in the knife boat until the entire ribbon sticks to the glass.
11. Remove the coverslip from the water and label it on one edge. Also, mark the position of the ribbon by circling it with a marker on the backside of the coverslip.

    This allows you to keep track of the samples and provides a way to tell which side of the coverslip the ribbon is mounted on (without a label, after the ribbon dries, it is not possible to tell which side it is on).
12. Let the ribbon dry at room temperature and place the coverslip on the slide warmer (~60°C) for 30 min. The slides can be stored at room temperature for at least 6 mo.

TROUBLESHOOTING

Problem (Step 8): The ribbons curve.

Solution: Sometimes, even when the leading and trailing edges of the blockface are parallel, the ribbons are curved. This can happen when there is more resin around the tissue on one side of the block than the other. As the section comes in contact with water it expands, however, the resin and tissue expand to different degrees, causing curving of the ribbon. Thus, make sure that the extra resin is trimmed on either side of the block.

Problem (Step 8): The ribbons break.

Solution: Trim the block using a very sharp razor blade or, even better, the Cryotrim diamond knife. Make sure that the blockface is at least twice as wide as it is high. Apply glue again and take care to align the block so the edge of the blockface is parallel to the knife edge.

Protocol C

Immunostaining and Antibody Elution

The tissue arrays are prepared for imaging by binding primary antibodies against specific cellular targets followed by secondary fluorescent antibodies. Alternatively, fluorescent proteins can be used that have been introduced into the tissue before dissection.

MATERIALS

CAUTION: See Appendix 6 for proper handling of materials marked with <!>.
See the end of the chapter for recipes for reagents marked with <R>.

Reagents

Alternative antibody dilution solution with normal goat serum (NGS) <R>
Alternative blocking solution with NGS <R>
Blocking solution with bovine serum albumin (BSA) <R>
Elution solution <R>
Glycine
Mounting medium: SlowFade Gold antifade reagent with DAPI <!> (Invitrogen S36939) or without DAPI (Invitrogen S36937)
Primary antibodies, see Table 1
A detailed list of antibodies that have been tested for array tomography is available from www.smithlab.stanford.edu.
Secondary antibodies: for example, the appropriate species of Alexa Fluor 488, 594, and 647, IgG (H+L), highly cross-adsorbed (Invitrogen)
Tissue sectioned as in Protocol B
Tris buffered saline tablets (Sigma-Aldrich T5030)

Equipment

Microcentrifuge
Microscope slides (precleaned Gold Seal Rite-On micro slides; Fisher Scientific 12-518-103)
PAP pen (ImmEdge Pen, Vector Laboratories H-4000)
Petri dishes, 100-mm diameter

TABLE 1. Primary antibodies used with array tomography

Antibody	Source	Supplier	Dilution
Synapsin I	Rabbit	Millipore AB1543P	1:100
PSD95	Mouse	NeuroMabs 75-028	1:100
VGluT1	Guinea pig	Millipore AB5905	1:1000
GAD	Rabbit	Millipore AB1511	1:300
Gephyrin	Mouse	BD Biosciences 612632	1:100
Tubulin	Rabbit	Abcam ab18251	1:200
Tubulin	Mouse	Sigma-Aldrich T6793	1:200
Neurofilament 200	Rabbit	Sigma-Aldrich N4142	1:100

Slide warmer set at 60°C
Transfer pipettes, extra fine-tip polyethylene (Fisher Scientific 13-711-31)

EXPERIMENTAL METHOD

1. Encircle the ribbon of sectioned tissue with a PAP pen.
2. Place the coverslip into a humidified 100-mm Petri dish and treat the sections with 50 mM glycine in Tris buffer for 5 min.
3. Apply blocking solution with BSA for 5 min.

   If there is a problem with high background staining, see the alternate blocking and staining protocol beginning with Step 21.
4. Dilute the primary antibodies in blocking solution with BSA. Approximately 150 µL of solution will suffice to cover a 30-mm-long ribbon.
5. Centrifuge the antibody solution at 13,000 revolutions per minute (rpm) for 2 min before applying it to the sections.
6. Incubate the sections in primary antibodies either overnight at 4°C or for 2 h at room temperature.

   Primary antibodies are diluted to 10 µg/mL, although the best concentration will need to be determined for each antibody solution.
7. Rinse the sections three to four times with Tris buffer for a total of ~20 min. Wash the sections using a manual "perfusion" method, simultaneously adding Tris buffer on one end and removing if from another with plastic transfer pipettes.
8. Dilute the appropriate secondary antibodies in blocking solution with BSA (1:150 for Alexa secondaries).
9. Centrifuge secondary antibody solution at 13,000 rpm for 2 min.
10. Incubate the sections in secondary antibodies for 30 min at room temperature in the dark.
11. Rinse the sections three to four times with Tris buffer for ~5 min each.
12. Wash the coverslip thoroughly with filtered ultrapure H_2O to remove any dust or debris, leaving some H_2O on the sections so that they do not dry out.
13. Mount the sections on a clean, dust-free microscope slide with SlowFade Gold Antifade containing DAPI.
14. Image the sections as soon as possible after immunostaining, or at least the same day. If you are planning to restain the sections with additional antibodies, elute the antibodies (Steps 15–19) as soon as possible after imaging.

Elute Antibodies Before Restaining

15. Add filtered ultrapure H_2O around the edge of the coverslip to help slide it off the microscope slide.

    Wash the coverslip gently with filtered ultrapure H_2O to rinse off the mounting medium.
16. Apply elution solution for 20 min.
17. Gently rinse the coverslips twice with Tris, allowing them to sit for 10 min with each rinse.
18. Rinse the coverslips with filtered ultrapure H_2O and let them air dry completely.
19. Bake the coverslip on a slide warmer set to 60°C for 30 min.

Staining the Sections Multiple Times

20. Restain using the Steps 2–13 above or store array at room temperature until needed.
    See *Troubleshooting*.

Alternative Staining Method to Reduce Background

21. Proceed through Steps 1 and 2 of the staining protocol above.
22. Incubate the sections for 30 min with alternative blocking solution with NGS.
    If secondary antibodies are made in donkey, use normal donkey serum; if secondary antibodies are made in horse, use normal horse serum, etc. This protocol can only be used if all of the secondary antibodies are made in the same animal.
23. Dilute the primary and secondary antibodies in alternative antibody dilution solution with NGS.
24. Follow the rest of the staining protocol above, using the solutions with NGS.

TROUBLESHOOTING

Problem (Step 20): There is incomplete elution of antibodies.

Solution: To check for incomplete elution, which could interfere with subsequent antibody staining, perform the following control experiment. Stain with the antibody of interest and image a region that you can relocate later. Elute and apply the secondary antibody again. Image the same region as before, using the same exposure time; this will give an estimate of how much primary antibody was left after the elution. Increase the exposure time to determine if longer exposure times reveal the initial pattern of antibody staining. If the first antibody was not eluted sufficiently, try longer elution times. Some antibodies elute poorly (e.g., rabbit synapsin or tubulin) and, if followed by a weaker antibody, may still be detectable after the elution. In such cases, begin the experiment with the weaker antibodies.

Protocol D

Imaging Stained Arrays

Tissue arrays are imaged using a conventional wide-field fluorescence microscopy. Images can be captured manually or, with the appropriate software and hardware, the process can be automated.

MATERIALS

Reagents

Immunostained brain sections prepared as in Protocol C

Equipment

Digital camera (Axiocam HR, Carl Zeiss)
Fluorescence filters sets (all from Semrock) YFP, 2427A; GFP, 3035B; CFP, 2432A; Texas Red, 4040B; DAPI, 1160A; FITC, 3540B; and Cy5, 4040A
Illuminator series 120 (X-Cite)
Objective (Zeiss Immersol 514 F Fluorescence Immersion Oil)
Piezo Automated Stage (Zeiss)
10× Plan-Apochromat 0.45 NA
63× Plan-Apochromat 1.4 NA oil objective
Software (e.g., Zeiss Axiovision with Interactive Measurement Module, Automeasure Plus Module and Array Tomography Toolbar; the toolbar can be downloaded from http://www.stanford.edu/~bbusse/work/downloads.html)
Upright microscope (Zeiss Axio Imager.Z1)

EXPERIMENTAL METHOD

Manual Image Acquisition

1. Focus on your sample using the 10× objective. Find the ribbon by focusing on the DAPI label or another bright label that is not prone to bleaching. Once you have found the right general area of the sample, switch to the 63× objective.

   See *Troubleshooting*.

2. Find the exact area of the sample that you want to image. Choose a landmark that you can use to find the same spot in the next section. A useful landmark should not change dramatically from one section to the next (e.g., a DAPI-stained nucleus or blood vessel). Because the sections are 70–200 nm thick we can often follow the same nucleus through the entire length of a long array. Line up your landmark with a crosshair in the middle of the field.
3. Set the correct exposure for each of your fluorescence channels.
4. Beginning with the first section, collect an image of your area of interest.
5. Manually, move to the same area of the next section. The glue on the edge of each section is autofluorescent, so you can tell when you have moved to the next section. Align your landmark carefully in each section to assure that your image alignment will run smoothly.

   See *Troubleshooting*.

6. Continue to the end of the ribbon, collecting an image from each section. Align your stack of images using Protocol E.

Automated Image Acquisition

Although we have developed our automated tools to work with Zeiss Axiovision software, any microscopy software suite (such as Micro-Manager) controlling an automated stage should be adaptable to this approach. Some steps may be altered or eliminated, depending on your framework and implementation.

7. With the 10× objective, find the ribbon by focusing on the DAPI label or another bright label that is not prone to bleaching.

   See *Troubleshooting*.

8. Acquire a mosaic image of the entire ribbon with the MosaicX Axiovision module, using a bright label that does not vary much between sections, such as DAPI.
9. Find the top left and bottom right corners of the ribbon and use them to define the limits of the mosaic in the Mosaic Setup dialog.
10. Set three to four focus positions along the length of the ribbon and enable focus correction.
11. Collect the mosaic image. Convert the mosaic to a single image with the "Convert Tile Images" dialog, setting the Zoom factor to 1 so that the resulting image is the same size.

    See *Troubleshooting*.

12. Choose a point of interest to be imaged in the ribbon. Place a marker on that point via Measure → Marker. Place another marker at the same spot in the next consecutive section. Create a table of the *x* and *y* coordinates of the markers, "DataTable," via Measure → Create Table, with the "list" option. This allows Axiovision's Visual Basic scripts to read the marker locations.

    See *Troubleshooting*.

13. With the large, stitched image selected, call "PrepImage" and "MarkLoop" from the Array Tomography toolbar.
14. The preceding step will create a file (csv) with a list of the coordinates for the same position in each section, which will be automatically saved in the same folder as the mosaic and with the same name as the stitched image. To load the position list, go to Microscope → Mark and Find, click the "New" icon, and then the "Import Position list" button. In the Mark and Find dialog, switch to the "Positions" tab which will let you review or edit the calculated positions by double-clicking on any position.
15. Collect one field of view at each point via Multidimensional Acquisition with the "position list" checkbox set. We recommend using a bright label that is present throughout the field as the first channel, setting it to autofocus at each position. Review your images at the end to make sure they are all in focus.

    See *Troubleshooting*.

TROUBLESHOOTING

Problem (Steps 1 and 7): Sections cannot be found under the microscope.

Solution: Use DAPI in the mounting medium—it will stain the nuclei brightly and make it easy to find the sections with the 10× objective. Make sure the coverslip has been mounted with the sections on the same side as the mounting medium and that there are no bubbles in the immersion oil.

Problem (Steps 5 and 15): Sections are wrinkled.

Solution: Section wrinkling can occur at several steps in the procedure. First, it can occur during array preparation if the coverslip is put on the slide warmer while the ribbon is still wet. Make sure that the sections are dry before putting them on the slide warmer. It can also occur if the blockface is too big (>1 × 2 mm) or sections are too thick (>200 nm). Second, wrinkles can be caused by improper subbing of the coverslips. The gelatin must be 300 Bloom (measure of stickiness, higher number indicates stickier) and should not be heated above 60°C during solution preparation. Third, sections can wrinkle if the ribbon is stored with the mounting solution for >2 d. Finally, wrinkling can occur after antibody elution, especially with sections 200 nm thick. Make sure that the solutions are applied gently during the elution and the array is completely dry before putting it on the slide warmer.

Problem (Steps 5 and 15): There is no staining or fluorescent signal.

Solution: Use a high-power, high-NA objective—ideally a 63× oil objective. Only immunofluorescence with antibodies against abundant antigens (e.g., tubulin, neurofilament) will be visible with a low-power objective. Also, check if there are two coverslips stuck to each other; this will make it impossible to focus at higher magnification.

Problem (Steps 5 and 15): Punctate staining is seen with a seemingly random distribution.

Solution: Immunostaining with thin array sections (≤200 nm) looks different from staining on thicker cryosections or vibratome sections. Because a very thin layer of tissue is probed, many stains that appear continuous on thicker sections will appear punctate with array tomography. A 3D reconstruction of a short ribbon (10–20 sections) can be helpful for comparison. You may also need to test antibody performance. First, compare the antibody staining pattern to that of different antibodies against the same antigen or a different antigen with a similar distribution. For example, a presynaptic marker should be adjacent to a postsynaptic marker. Other common controls for immunostaining can be used, such as omitting primary antibodies, staining a tissue that does not contain the antigen, etc. Second, specific controls for array tomography include comparison of the antibody staining patterns from adjacent sections or from consecutive stains (i.e., stain → image → elute → stain with the same antibody → image the same region → compare). Not all antibodies that work well for other applications will work for array tomography.

Problem (Steps 5 and 15): There is high background fluorescence.

Solution: Background fluorescence can have many causes. Often, there is high autofluorescence when using the low-power (but not high-power) objectives. If the autofluorescence levels are high with the 63× objective, try the following. First, check whether the immersion oil is designed to be used with fluorescence. Second, labeling marks on the back of the coverslip can dissolve in the immersion oil causing autofluorescence—wipe labels off with ethanol before imaging. Third, use high-quality fluorescence filter sets. Fourth, try a longer fluorescence quenching step (glycine treatment in Protocol C, Step 2), the alternative staining method (Protocol C, Step 21), or introduce an additional quenching step with 1% sodium borohydride in Tris buffer for 5 min.

Problem (Steps 5 and 15): Green fluorescent protein (GFP)/YFP fluorescence is lost.

Solution: First, confirm that the tissue was dehydrated only to 70% ethanol (Protocol A, Step 14). Second, make sure you are using a high-power, high-NA objective. To check for GFP fluorescence use a short array with ultrathin sections (<200 nm). Let it sit for 5–10 min or more with Tris-glycine (50 mM glycine in Tris), mount over a glass slide and look with the 63× objective. GFP can bleach very fast, so work quickly to find the region with GFP fluorescence. For acquiring images, select the region of interest with another stain (e.g., Alexa 594) and focus. Do not use the DAPI stain for this purpose, because it can cause DAPI to bleed into the GFP channel. In cases of weak GFP fluorescence, GFP antibodies may help identify GFP-positive cell bodies and large processes, but are generally not useful for thinner processes. GFP antibodies for array

tomography include Roche 11814460001 (mouse), MBL 70 (rabbit), Invitrogen A11122 (rabbit), NeuroMabs 75-131 (mouse), GeneTex GTX13970 (chicken). All of these antibodies should be used at 1:100 dilution.

Problem (Step 11): The "Convert Tile Images" step keeps downsampling the stitched image.
Solution: In the Tools → Options → Acquisition menu, change the Mx. MosaicX image size to the maximum allowed: 1000000000 pixel.

Problem (Step 12): The microscopy software is not designed for array tomography.
Solution: We have developed an algorithm that automates position finding in the arrays by using simple extrapolation to estimate the neighborhood of an unknown point and then refining the estimate with an autocorrelation search. Given two known points Pn and Pn−1, we find the next point Pn+1 such that Pn+1 = Pn + (Pn − [Pn−1]) (Fig. 4). This does not take into account ribbon curvature or changes in section width, but gives a rough approximation of the unknown point's locale. Pn+1 becomes the center of an autocorrelation search to find the point's true position. The size of the search varies with the width of the sections; larger sections will have larger warping and curvature effects, and any miscalculation in the estimate of Pn+1 will be magnified.

To conduct the search, the algorithm compares the area centered at Pn+1 with a Kalman-filtered image of recently processed points. Although our fiducial labels (DAPI and tubulin immunostaining) have minor variations from section to section, it does not disrupt the accuracy of the correlation search. To make the Kalman-filtered image at each iteration, use the area around the current Pn, *newSample*, to update the image using the following pseudocode: image = 0.3 × image + 0.7 × *newSample*. The purpose of using the Kalman filter, when *newSample* alone would do, is to add a measure of robustness to the algorithm. If the ribbon is damaged or has aberrant staining on a single section, using *newSample* alone may result in the algorithm going off course. With a running average of previous iterations to compare with, a defect in a single section has a good chance of being ignored. This process continues until one end of the ribbon is reached, then starts in the other direction.

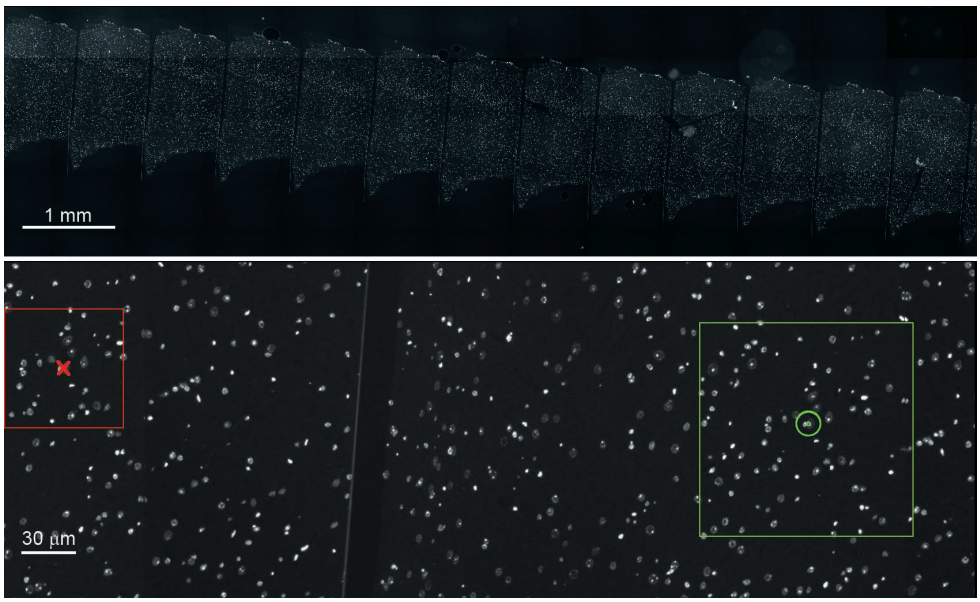

FIGURE 4. (*Top*) A fragment of an array tomography ribbon stained with DAPI. (*Bottom*) A closer view of two sections in the ribbon showing a single iteration of the position-finding algorithm. An established field (red x) is used to maintain a reference patch (red square) for a correlation-based search (green square) to find the next point (green circle).

We developed an implementation of this algorithm in Visual Basic script for Zeiss Axiovision, available from http://www.stanford.edu/~bbusse/work/downloads.html, and would welcome any ports to other microscopy software.

Problem (Step 15): Autofocus does not work using Axiovision.

Solution: The autofocus does not work every time. Typically, ~5% of the images collected with autofocus may be out of focus. In that case, you can move to the positions on the ribbon with bad focus, focus by hand, and collect individual images. Replace the out-of-focus images with the newly focused ones in the stack before to alignment. If 10% or more of the images are out of focus, you can try using the autofocus with a different channel. Pick a channel with antibody staining that is bright, and present throughout the field of view. Using a channel with dim or sparse immunostaining will not work well.

Problem (Step 15): Autofocus is grayed out.

Solution: In the Tools → Options → Acquisition menu, check the box marked either "Use calibration-free Autofocus" or "Enable new Autofocus."

Protocol E

Semiautomated Image Alignment

Successful array tomography requires that the captured images be properly stacked and aligned. Software to achieve these ends is freely available.

MATERIALS

Software

Fiji can be obtained at http://pacific.mpi-cbg.de/wiki/index.php/Main_Page
MultiStackReg is available at http://www.stanford.edu/~bbusse/work/downloads.html

EXPERIMENTAL METHOD

1. Load your images into Fiji. If using Axiovision, Fiji's Bio-Formats Importer plugin can read .zvi files directly.
2. Pick a channel that is relatively invariant from one section to the next (e.g., DAPI or tubulin), and select a slice near the middle of the ribbon.
3. Align the sections of that channel using "affine" in MultiStackReg (Fiji), but do not save over the misaligned stack. Save the resulting transformation matrix. This is the intrasession matrix.

   See *Troubleshooting*.
4. Using MultiStackReg, apply that matrix to the other channels of the same imaging session.
5. For each subsequent imaging session, choose the same channel. Align the new (misaligned) channel to the old (misaligned) channel, saving the matrix. This is the intersession matrix.
6. For each channel in that imaging session, first apply the intersession matrix from Step 5 and then the intrasession matrix from Step 3.
7. Repeat until all imaging sessions have been registered.

TROUBLESHOOTING

Problem (Step 3): The alignment steps are not working properly.

Solution: Detailed instructions with graphical illustration, compiled by Andrew Olson, are available at http://nisms.stanford.edu/UsingOurServices/Training.html. If an "affine" transformation does not align the images well, try either the "rigid body" then "affine" or try "rigid body" alone. For each registration step, save the transformation matrix and apply it to the other channels in sequence.

MultiStackReg is an extension of the StackReg ImageJ plugin, which is dependent on TurboReg (Thévenaz et al. 1998). TurboReg aligns a single pair of images using a pyramid registration scheme. StackReg aligns an entire stack by calling TurboReg on each pair of consecutive slices in the stack, propagating the alignment to later slices. The two principle changes added by

MultiStackReg are the ability (1) to load and save transformation matrices and (2) to align one stack to another by registering each pair of corresponding sections independently. MultiStackReg can process TurboReg alignment files in the same manner as the files it generates for itself, so if your alignment is failing owing to a single section, it is possible to manually align that section in TurboReg, apply that transform to a copy of the stack, and splice the two together.

CONCLUSION AND FUTURE DIRECTIONS

One important application of array tomography in the field of neuroscience is the analysis of synapse populations. With this method it is possible to resolve individual synapses in situ within brain tissue specimens. Because 10 or more antibodies can be used on an individual sample, the molecular signature of each synapse can be defined with unprecedented detail. The throughput of the technique is inherently high, approaching the imaging of one million synapses per hour. Compared with 3D reconstruction at the electron microscopic level, array tomography can image much larger volumes and provide information about the presence of a much larger number of molecules, but cannot presently provide the fine ultrastructure of electron microscopy. On the other hand, the amount of effort involved in array tomography may not be warranted for all studies. If it is not considered critical to resolve individual synapses, immunostaining of vibratome sections or cryosections and confocal microscopy imaging may be sufficient.

Currently, we are focused on developing array tomography in three directions. First, we are refining current staining and imaging approaches to image larger and larger tissue volumes with more antibodies. Second, we are combining light and electron microscopic imaging to visualize both immunofluorescence and ultrastructure on the same tissue sections. Finally, we are applying advanced computational methods for data analysis, in particular with the goal to both count and classify millions of synapses on a routine basis.

RECIPES

CAUTION: See Appendix 6 for proper handling of materials marked with <!>.
Recipes for reagents marked with <R> are included in this list.

Alternative Antibody Dilution Solution with NGS (1 mL)

Reagent	Quantity	Final concentration
Tween (1%) (make the stock solution using Tween-20 [Electron Microscopy Sciences 25564])	100 µL	0.1%
NGS (Invitrogen PCN5000)	30 µL	3%
Tris buffer	870 µL	

Prepare on the same day it is used. NGS can be kept frozen in aliquots for several months.

Alternative Blocking Solution with NGS (1 mL)

Reagent	Quantity	Final concentration
Tween (1%) (make the stock solution using Tween-20 [Electron Microscopy Sciences 25564])	100 µL	0.1%
NGS (Invitrogen PCN5000)	100 µL	10%
Tris buffer	800 µL	

Prepare on the same day it is used. NGS can be kept frozen in aliquots for several months.

Blocking Solution with BSA (1 mL)

Reagent	Quantity	Final concentration
Tween (1%) (make the stock solution using Tween-20 [Electron Microscopy Sciences 25564])	50 µL	0.05%
BSA (10%) (AURION BSA C [acetylated BSA], Electron Microscopy Sciences 25557)	10 µL	0.1%
Tris buffer	940 µL	

Prepare the same day. The 1% Tween stock (10 µL Tween in 1 mL of H_2O) and the 10% BSA stock can be kept at 4°C for several months.

Elution Solution (10 mL)

Reagent	Quantity	Final concentration
NaOH <!>, 10 N	200 µL	0.2 N
SDS <!> (20%)	10 µL	0.02%
Distilled H_2O	10 mL	

Can be prepared in advance and stored at room temperature for several months.

Fixative (4 mL)

Reagent	Quantity	Final concentration
Paraformaldehyde <!> (8%, EM grade; Electron Microscopy Sciences 157-8)	2 mL	4%
PBS, 0.02 M (use PBS powder, pH 7.4 [Sigma-Aldrich P3813])	2 mL	0.01 M
Sucrose	0.1 gm	2.5%

Prepare the same day as it will be used.

Subbing Solution (300 mL)

Reagent	Quantity	Final concentration
Gelatin from porcine skin, 300 Bloom (Sigma-Aldrich G1890)	1.5 g	0.5%
Chromium potassium sulfate (Sigma-Aldrich 243361)	0.15 g	0.05%
Distilled H_2O	300 mL	

Prepare the same day. Dissolve the gelatin in 290 mL of distilled H_2O by heating to <60°C. Dissolve 0.15 gm of chromium potassium sulfate in 10 mL of H_2O. When the gelatin solution cools down to ~37°C, combine the two solutions, filter, and pour into the staining tank. Use fresh.

Wash Buffer (50 mL)

Reagent	Quantity	Final concentration
Glycine	187.5 mg	50 mM
Sucrose	1.75 g	3.5%
PBS, 0.02 M	25 mL	0.01 M
Distilled H_2O	25 mL	

Can be prepared in advance and stored at 4°C for up to 1 mo; discard if it appears cloudy.

ACKNOWLEDGMENTS

We thank JoAnn Buchanan and Nafisa Ghori for their help in refining the methods. This work was supported by grants from McKnight Endowment Fund for the Neurosciences, the National Institutes of Health (NS 063210), The Gatsby Charitable Foundation, and the Howard Hughes Medical Institute.

REFERENCES

Feng G, Mellor RH, Bernstein M, Keller-Peck C, Nguyen QT, Wallace M, Nerbonne JM, Lichtman JW, Sanes JR. 2000. Imaging neuronal subsets in transgenic mice expressing multiple spectral variants of GFP. *Neuron* **28:** 41–51.

Koffie RM, Meyer-Luehmann M, Hashimoto T, Adams KW, Mielke ML, Garcia-Alloza M, Micheva KD, Smith SJ, Kim ML, Lee VM, et al. 2009. Oligomeric amyloid β associates with postsynaptic densities and correlates with excitatory synapse loss near senile plaques. *Proc Natl Acad Sci* **106:** 4012–4017.

Micheva KD, Smith SJ. 2007. Array tomography: A new tool for imaging the molecular architecture and ultrastructure of neural circuits. *Neuron* **55:** 25–36.

Smith SJ. 2007 Circuit reconstruction tools today. *Curr Opin Neurobiol* **17:** 601–608.

Stevens B, Allen NJ, Vazquez LE, Howell GR, Christopherson KS, Nouri N, Micheva KD, Mehalow A, Huberman AD, Stafford B, et al. 2007. The classical complement cascade mediates CNS synapse elimination. *Cell* **131:** 1164–1178.

Thévenaz P, Ruttimann UE, Unser M. 1998. A pyramid approach to subpixel registration based on intensity. *IEEE Trans Image Process* **7:** 27–41.